Mon. Not. R. Astron. Soc. **299,** 349–356 (1998)

Mass constraints from multiphase cooling flow models

Peter A. Thomas

Astronomy Centre, School of Chemistry, Physics and Environmental Science, University of Sussex, Falmer, Brighton BN1 9QH

Accepted 1998 March 18. Received 1998 March 11; in original form 1996 October 11

ABSTRACT

I review the multiphase cooling flow equations that reduce to a relatively simple form for a wide class of self-similar density distributions described by the single parameter, k, first introduced by Nulsen. It is shown that steady-state cooling flows are *not* consistent with all possible emissivity profiles, which can therefore be used as a test of the theory. In combination, they provide strong constraints on the temperature profile and mass distribution within the cooling radius. The model is applied to *ROSAT* HRI data for three rich clusters. At one extreme ($k \sim 1$) these show evidence for cores in the mass distribution of size $110–140\,h_{50}^{-1}$ kpc and have temperatures that decline towards the flow centre. At the other ($k \mapsto \infty$), the mass density and gas temperature both rise sharply towards the flow centre. The former are more consistent with observations which usually show a lower emission-weighted temperature within the cooling flow than from the cluster as a whole. The requirement that the solutions have a temperature gradient that is non-increasing towards the cluster centre limits the matter density gradient to be shallower than $\rho_{\rm grav} \propto r^{-1.2}$ in the cluster core.

Key words: cooling flows – dark matter.

1 INTRODUCTION

The multiphase nature of the intracluster medium (ICM) in cooling flows was demonstrated a decade ago when deprojections of X-ray surface brightness profiles showed that mass cools and is deposited from the flow in a distributed manner, $\dot{M} \propto r$ (e.g. Thomas, Fabian & Nulsen 1987). However, the complexity of the theory and lack of data with high spatial resolution mean that the single-phase approximation is still widely adopted. In this paper I show how the use of self-similar density distributions can lead to a relatively simple form for the multiphase cooling flow equations whilst spanning the whole range of expected behaviours in the more general case. In combination with the emissivity profile (for a spherically symmetric flow), the equations can be solved to yield the gas temperature and mass profiles within the cooling flow.

In Section 2, I introduce the concept of the volume fraction to describe the distribution of density phases in the ICM. The self-similar forms of the volume fraction are determined and shown to span all reasonable behaviours for the more general situation. The steady-state, self-similar form of the cooling flow equations is derived in Section 3, and it is shown how these can be solved in the spherically symmetric case if the emissivity profile is known. The behaviour of the solutions is examined in detail: not every emissivity profile is consistent with these models. In Section 4, the theory is applied to *ROSAT* High Resolution Imager (HRI) data for three clusters with some success. Finally, the results are summarized and further discussed in Section 5.

2 THE FORM OF THE DENSITY DISTRIBUTION

The theory of multiphase cooling flows was set out by Nulsen (1986, 1988). He introduced the concept of the volume fraction, $f(\rho, \boldsymbol{r}, t)$, such that $f\,{\rm d}\rho$ is the fractional volume occupied by phases with densities in the range ρ to $\rho + {\rm d}\rho$. It is assumed that the phases comove but are thermally isolated from one another – these can be regarded as empirical facts as otherwise the flow would rapidly evolve to a single-phase state.

Given these assumptions then it is relatively straightforward to derive an equation for the evolution of the volume fraction (see the Appendix). Writing

$$f = \frac{(2-\alpha)}{\rho_0} w^{(4-\alpha)/(2-\alpha)} g(w, \boldsymbol{r}, t), \tag{1}$$

where

$$w = \left(\frac{\rho_0}{\rho}\right)^{2-\alpha} \tag{2}$$

and $\rho_0 = \rho_0(\boldsymbol{r}, t)$, then

$$\frac{\dot{g}}{g} + (3-\alpha)\frac{\dot{\rho}_0}{\rho_0} - \frac{2-\alpha}{\gamma}\frac{\dot{P}}{P} + \nabla\cdot\boldsymbol{u} = 0, \tag{3}$$

where the dot refers to a covariant derivate, following the flow.

In general g is a complicated function of position and time. However, we can look for solutions in which g has a constant functional form, $g = g(w)$. Only the first term in equation (3) depends upon w. Hence we require that $\dot{g} \equiv \dot{w}\,{\rm d}g/{\rm d}w \propto g$. There are two kinds of solution.

(i) $g = g_\infty \propto \exp(-w)$. This is the most extended distribution which is convectively stable (it gives $P \propto \rho_0^\gamma$). It includes phases of arbitrarily low density.

(ii) $g = g_k \propto (1-w)^{k-1}$, $0 < w < 1$; $k \geq 1$. These solutions possess a minimum density, $\rho \geq \rho_0$. $k = 1$ is the least extended, consisting solely of the power-law cooling tail. As $k \mapsto \infty$ the solutions resemble g_∞.

For other forms of g one must resort to numerical integration to follow their evolution. Thomas (1988b) looked at the steady-state evolution of a range of distributions with a sharp cut-off at low densities, and reached the following conclusions.

(1) All distributions develop a high-density tail, $f \sim \rho^{-(4-\alpha)}$, as they cool.

(2) Sufficiently narrow distributions resemble the pure power-law g_1 by the time they begin to be deposited.

Waxman & Miralda-Escudé (1995) showed that the self-similar models give good approximations to more general behaviour, provided that most of the gas is initially within a distribution that resembles g_k over some finite density range (it is not necessary to reproduce the whole distribution). Given the variety of functional forms generated by different values of k, this is not at all unlikely.

g_1 and g_∞ bound all reasonable solutions of the cooling flow equations, be they self-similar in form or not. In principle, k could be less than unity (as $k \mapsto 0$ the flow tends to the homogeneous case) but it is difficult to see how such distributions could arise. If the large density variations inferred within the cooling radius result from amplification of an initially much narrower distribution, then values of k of order unity are to be preferred. Without a plausible formation history for the ICM, however, it is better to leave k as a free parameter to be determined empirically. I will argue below that low values of k fit the observations of cooling flows in rich clusters better than high values.

3 RECONSTRUCTION OF CLUSTER MASS PROFILES

The self-similar density distributions derived in Section 2 lead to particularly simple forms of the steady-state cooling flow equations. I derive these below and then show in the next section how they can be combined with the emissivity profile to provide strong constraints of the mass distribution within the cooling radius.

Equivalent equations were first derived by Nulsen (1986) who considered power-law solutions. Thomas et al. (1987) used this model to 'deproject' several well-resolved cooling flows, and showed that one recovered density distributions with a cooling tail, $f \propto \rho^{-(4-\alpha)}$, only if an extended halo was added to the potential of the central galaxy. Similarly, Waxman & Miralda-Escudé (1995) fixed the mass and emissivity profiles, then searched for the corresponding density distribution, $f(\rho)$. In this paper we take a slightly different approach: we assume a form for $f(\rho)$, then derive the mass profile.

3.1 The equations

Substituting the functional form of g_k into equations (A2), (A3) and (3), we see that the self-similar forms of the cooling flow equations are

$$\frac{\dot\rho_0}{\rho_0} - \frac{1}{\gamma}\frac{\dot P}{P} - \frac{\beta}{(2-\alpha)k} = 0 \tag{4}$$

and

$$\frac{\dot\rho_0}{\rho_0} + \nabla\cdot\boldsymbol{u} + \beta = 0, \tag{5}$$

where

$$\beta = (2-\alpha)k\frac{\gamma-1}{\gamma}\frac{n_0^2\Lambda(T_0)}{P}. \tag{6}$$

To these may be added the equation of hydrostatic support,

$$\nabla\Phi + \frac{\nabla P}{\bar\rho} = 0, \tag{7}$$

where Φ is the gravitational potential. I assume here that the inflow is subsonic – this turns out to be a good approximation in all multiphase cooling flow models.

In a steady-state and spherical symmetry the above equations reduce to

$$\frac{\mathrm{d}\ln P}{\mathrm{d}\ln r} = -2\Sigma, \tag{8}$$

$$\frac{\mathrm{d}\ln\bar\rho}{\mathrm{d}\ln r} = -\frac{2}{\gamma}\Sigma - \frac{\tau}{2-\alpha} \tag{9}$$

and

$$\frac{\mathrm{d}\ln u}{\mathrm{d}\ln r} = -2 + \frac{2}{\gamma}\Sigma + \left(\frac{1}{2-\alpha}+k\right)\tau, \tag{10}$$

where

$$\Sigma = \frac{GM}{2r}\frac{\mu m_\mathrm{H}}{k_\mathrm{B}T} \tag{11}$$

is the ratio of the virial and the thermal temperatures, and

$$\tau = (2-\alpha)\frac{\gamma-1}{\gamma}\frac{n_0^2\Lambda(T_0)}{P}\frac{r}{u} = \frac{1}{k}\frac{\mathrm{d}\ln\dot M}{\mathrm{d}\ln r} \tag{12}$$

is the ratio of the inflow time to the constant-pressure cooling time.

Although there appear to be three equations here, the dimensionless ratios Σ and τ are the only important variables. The third equation merely acts as a scaling (for fixed τ, $\bar\rho^{2-\alpha} \propto p^{1-\alpha}u$). Hence the physics can be captured in just two equations:

$$\frac{\mathrm{d}\ln\Sigma}{\mathrm{d}\ln r} = \chi - 1 + 2\frac{\gamma-1}{\gamma}\Sigma - \frac{\tau}{2-\alpha} \tag{13}$$

and

$$\frac{\mathrm{d}\ln\tau}{\mathrm{d}\ln r} = 3 - \frac{2}{\gamma}\left[(3-\alpha)-\gamma(1-\alpha)\right]\Sigma - \left(\frac{3-\alpha}{2-\alpha}+k\right)\tau, \tag{14}$$

where $\chi \equiv \mathrm{d}\ln M/\mathrm{d}\ln r$. The g_∞ equations can be recovered by letting $k \mapsto \infty$ and using $k\tau$ in place of τ as the second dimensionless variable.

The usual way of proceeding when solving the single-phase equations is to pick a functional form for the mass profile, χ, and mass deposition rate, β, then to solve for Σ and τ. From this one can generate an emissivity profile, $\xi(r)$, for comparison with the data. Here I adopt a different approach: because in the multiphase models β is fixed (for a particular value of k), one can specify $\xi(r)$ and *determine* the mass profile.

Suppose that $\beta_\mathrm{fit} \equiv -(1/6)\mathrm{d}\ln\xi/\mathrm{d}\ln r$ is known. Then

$$\frac{\mathrm{d}\ln\tau}{\mathrm{d}\ln r} = 3 - 6\frac{(3-\alpha)-\gamma(1-\alpha)}{2-\alpha+\alpha\gamma}\beta_\mathrm{fit} - \left[\frac{2\gamma}{(2-\alpha)(2-\alpha+\alpha\gamma)}+k\right]\tau. \tag{15}$$

Furthermore, this is an eigenvalue problem: requiring that the solution extend to $r = 0$ fixes the outer boundary condition. Hence we can solve for τ, Σ and χ.

The solution predicts a temperature profile for the cooling flow. Where spatially resolved spectra are available, this may allow k to be determined.

3.2 The behaviour of solutions

We can get a good idea of the behaviour of the solutions to equation (15) by looking at the case of constant $\beta_{\rm fit}$. Imposing the physical constraints $\Sigma \geq 0$ (i.e. a non-negative temperature) and $\chi \geq 0$ (i.e. mass constant or increasing with radius) restricts $\beta_{\rm fit}$ to lie in the range

$$\frac{3}{2(5+3k)} \leq \beta_{\rm fit} \leq \frac{80+21k}{120+36k} \qquad (16)$$

(in this expression and henceforth I set $\gamma = 5/3$ and $\alpha = 0.5$ rather than including them explicitly). Thus steep emissivity profiles, $\beta_{\rm fit} > 0.65$, are incompatible with all steady-state cooling flow models (larger values can occur, however, outside the cooling radius). In addition, the inner value of $\beta_{\rm fit}$ can be used to constrain k: flat cores are inconsistent with small values of k and a central decrease in emissivity would be incompatible with all models. If we assume that the virial temperature drops (i.e. $\Sigma \mapsto 0$) within the cluster core, then the central value of $\beta_{\rm fit}$ provides a *measure* of k.

The numerical solutions of equation (15) in the case of non-constant $\beta_{\rm fit}$ are illustrated in Fig. 1. Here I have set $\beta_{\rm fit} = 0.6 + 0.1 \log_{10} r$ and $k = 1$. Panel (a) shows the speed at which solutions diverge away from the desired one (i.e. the one that extends to $r = 0$) as r decreases. This ensures that the solutions are insensitive to the inner boundary condition and are stable to small variations in the value of $\beta_{\rm fit}$ in the inner bin (which is most likely to be affected by the point-spread function, uncertain absorption correction, etc.). The difference in the two values of τ at $r = 10^{-3}$ in the figure is less than 1 per cent. Panel (b) shows that the solutions are able to cope with quite large variations in $\beta_{\rm fit}$: in this case 100 fluctuations drawn from a uniform distribution of extent ± 0.1 have been added to each decade in r. Despite the fact that $\beta_{\rm fit}$ now varies outside both ends of the physical range described in equation (16), it remains true to the smooth solution. In this paper we will fit smooth functions to observed emissivity profiles before attempting to solve the cooling flow equations.

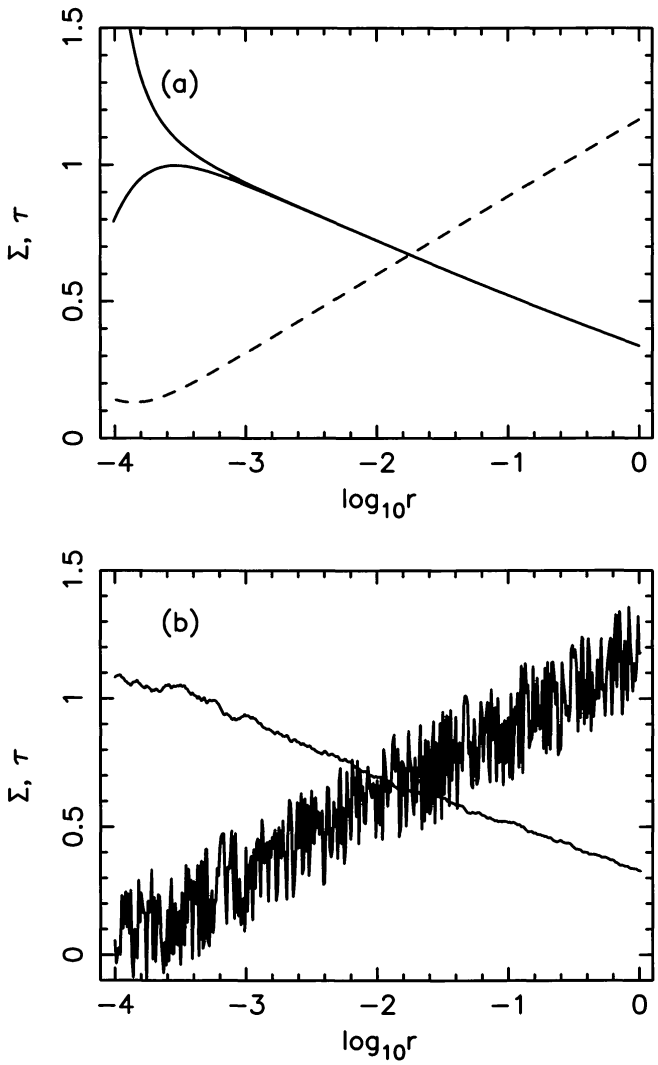

Figure 1. Solutions to the multiphase cooling flow equation, equation (15), for simple test profiles: (a) $\beta_{\rm fit} = 0.6 + 0.1 \log_{10} r$, (b) $\beta_{\rm fit} = 0.6 + 0.1 \log_{10} r \pm 0.1$. The curves that decline and increase with radius represent solutions for τ and Σ, respectively.

4 APPLICATION TO RICH CLUSTERS

I will now apply the above theory to three cooling flow clusters: A85, PKS 0745−191 and A2029. The *ROSAT* HRI data were kindly supplied to me by Clovis Peres in the form of deprojected density and temperature profiles. This has the advantage that conversion of the counts into emissivity, including correction for the spectral response and absorption, has already been included. Provided that the cooling flow solutions resemble the deprojected one, then these corrections will hold good.

The deprojected data contain only predicted temperature profiles. Actual measures of the temperature profiles of clusters can provide strong constraints on the models and I will discuss the observations below, before applying the multiphase models to each of the clusters in turn.

4.1 Temperature profiles

There are only a few clusters with spatially resolved temperatures, mainly from *ASCA*. The evidence is slightly confusing because, although they show lower temperatures in the cluster cores than elsewhere, when fitted with a multiphase model the upper temperature of the gas in the core is similar to that in the cluster as a whole.

Consider the data on PKS 0745−191 (Allen, Fabian & Kneib 1996a). The *ASCA* data show a 'consistent trend of increasing temperature with radius' when fitted with single-temperature spectra. When a cooling flow is added to the model, however, it is possible to obtain a fit in which the ambient cluster temperature is approximately constant with radius, but with a greater mass deposition rate in the centre. In this analysis, however, the relative contributions to the emission from the ambient ICM and the cooling flow are arbitrary. Allen et al. also consider a single-phase deprojection of the *ROSAT* data in which they *assume* the temperature to be isothermal and deduce a mass profile for the cluster with either a small core radius, or equivalently a large contribution from the central cluster galaxy.

Similarly, observations of other massive cooling flows (Allen et al. 1996b) give similar results: the emission-weighted temperature declines towards the cluster core, but the observations are consistent with a variable mass deposition rate from a constant-temperature ICM.

It would be extremely useful to determine the temperature profile across the cooling flow region itself, but unfortunately cooling radii

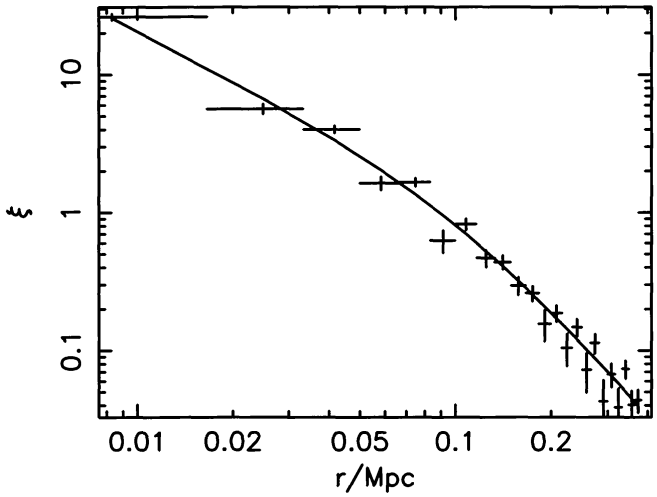

Figure 2. The emissivity profile for A85 in 12-arcsec bins. The solid line shows a broken power-law fit as described in the text.

are typically too small even for *ASCA* to be able to resolve them.

4.2 A85

The emissivity profile is shown in Fig. 2. There are 23 annular bins, each 12 arcsec wide, of which the inner nine have cooling times less than 1.33×10^{10} yr (throughout this paper I take $H_0 = 50\,\mathrm{km\,s^{-1}Mpc^{-1}}$). The profile is well-fitted by a simple broken power-law,

$$\xi \propto \left[\left(\frac{r}{0.12\,\mathrm{Mpc}}\right)^{1.18} + \left(\frac{r}{0.12\,\mathrm{Mpc}}\right)^{2.83}\right]^{-1}. \qquad (17)$$

The asymptotic slope of ξ as $r \mapsto 0$ is very close to the minimum permitted for $k = 1$ (see equation 16), which suggests that the solution will require an inner core in the mass distribution. This is illustrated in Fig. 3. Note that Σ drops very close to zero at $r = 10\,\mathrm{kpc}$ (it tends to a small constant value within this radius). The gravitational density profile (i.e. that of the total mass, not just the gas) is well-fitted at radii greater than 20 kpc by a King model,

$$\rho_{\mathrm{grav}} \propto \left[1 + \left(\frac{r}{0.11\,\mathrm{Mpc}}\right)^{2}\right]^{-1.25}. \qquad (18)$$

Within this radius the density is poorly constrained. Although it appears to rise, only a small change in the slope of ξ would cause it to level off or even fall – all we know for sure is that the virial temperature becomes very small. Note also that there is only one bin within 20 kpc and this one is most likely to be affected by smoothing by the point-spread function, uncertain correction for excess absorption, etc.

Note that the slope of the mass deposition profile, τ, is close to unity within the cooling radius, $r_{\mathrm{cool}} \approx 150$ kpc. This radius is not a special one for our solutions, as we have assumed that the cooling flow solution holds everywhere. For this reason the asymptotic slope of the gravitational density profile at larger radii should be taken with a pinch of salt.

The temperature of the gas is approximately constant outside the core radius, but drops by a factor of 5 in to 10 kpc. The emission-weighted temperature within 50 kpc is 51 per cent of that between 50 and 150 kpc (beyond that radius our steady-state solution may not be valid but it suggests that the gas is approximately isothermal). This is consistent with *ROSAT* spectra: although they cannot rule out a uniform temperature of about 4 keV, Pislar et al. (1997) find

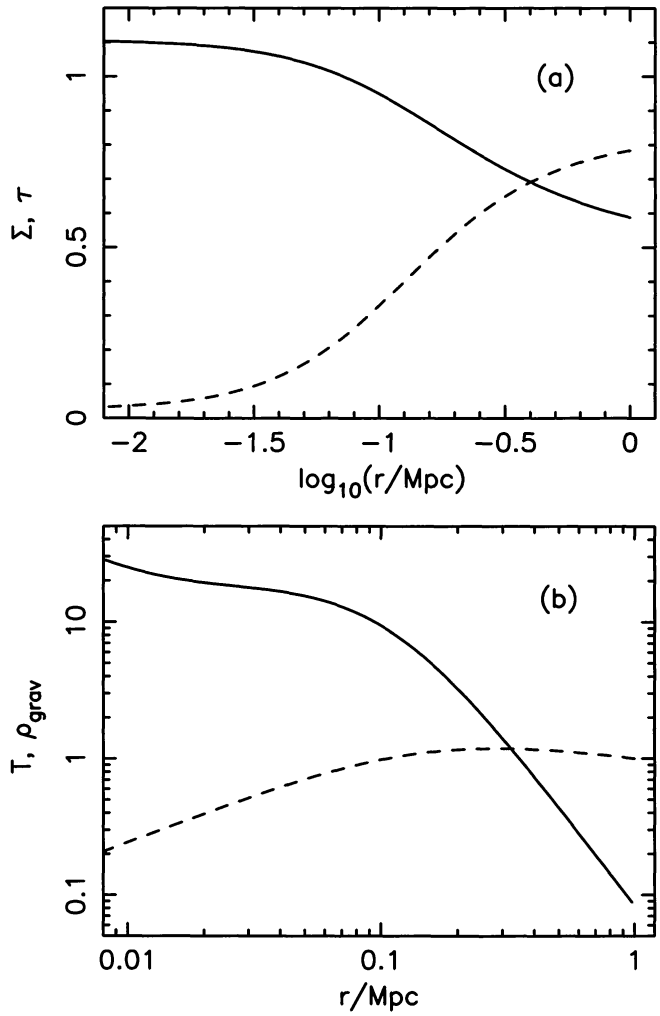

Figure 3. The $k = 1$ cooling flow solution for A85: (a) Σ (dashed line) and τ (solid line), (b) the density of the gravitating matter (solid line) and the gas temperature (dashed line), in arbitrary units.

strong evidence for a lower temperature of about 2.8 keV for the emission within a *projected* radius of 50 kpc of the cluster centre.

The solution for $k = \infty$ is shown in Fig. 4. There is no core in the gravitational mass profile in this case, with ρ_{grav} rising as r^{-2} all the way in to 10 kpc. This is reflected in the temperature profile: the gas temperature at 10 kpc is 10 times that at 1 Mpc, and the emission-weighted temperature within 50 kpc is 2.5 times that in the range 50–150 kpc. The observations by Pilsner et al., mentioned above, would seem to rule out such an extreme temperature rise in the cluster centre.

If the temperature is required to be approximately constant within the cooling radius, then $k = 3$ and the matter density profile rises as $\rho_{\mathrm{grav}} \propto r^{-1.3}$ within the inner 100 kpc.

4.3 PKS 0745–191

The emissivity profile, shown in Fig. 5, has 19 bins of width 8 arcsec, with 9–12 bins interior to the cooling radius ($r_{\mathrm{cool}} \approx 180$–240 kpc). The first thing to note is that ξ flattens considerably in the innermost bin. This is incompatible with density distributions with small values of k. In fact the fit shown by the solid line,

$$\xi \propto \left[1 + \left(\frac{r}{31\,\mathrm{kpc}}\right)^{2.28} + \left(\frac{r}{89\,\mathrm{kpc}}\right)^{4.09}\right]^{-1}, \qquad (19)$$

admits solutions that extend to $r = 0$ only for $k = \infty$ (Fig. 6).

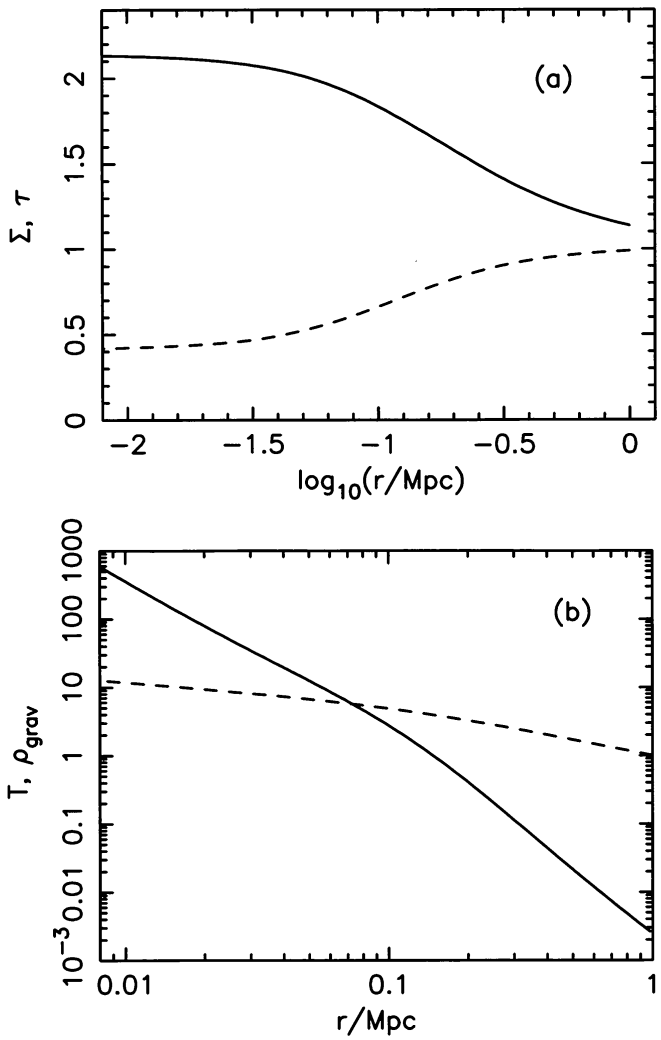

Figure 4. The $k = \infty$ cooling flow solution for A85: (a) Σ (dashed line) and τ (solid line), (b) the density of the gravitating matter (solid line) and the gas temperature (dashed line), in arbitrary units.

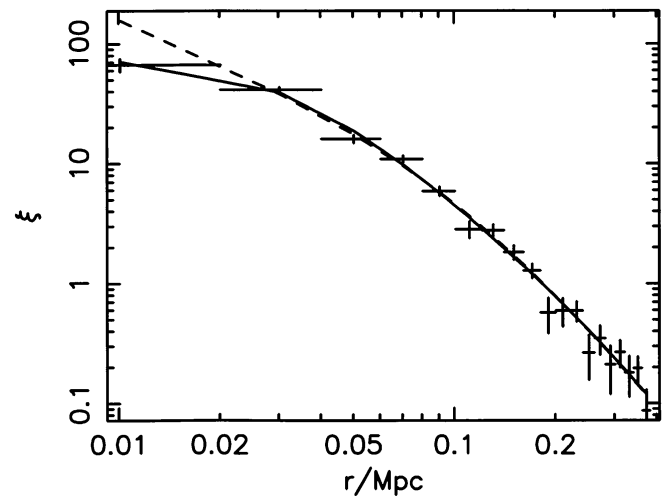

Figure 5. The emissivity profile for PKS 0745–191 in 8-arcsec bins. The solid line shows an analytic fit to the data and the dashed line shows the emissivity profile corresponding to a King-law density profile, as described in the text.

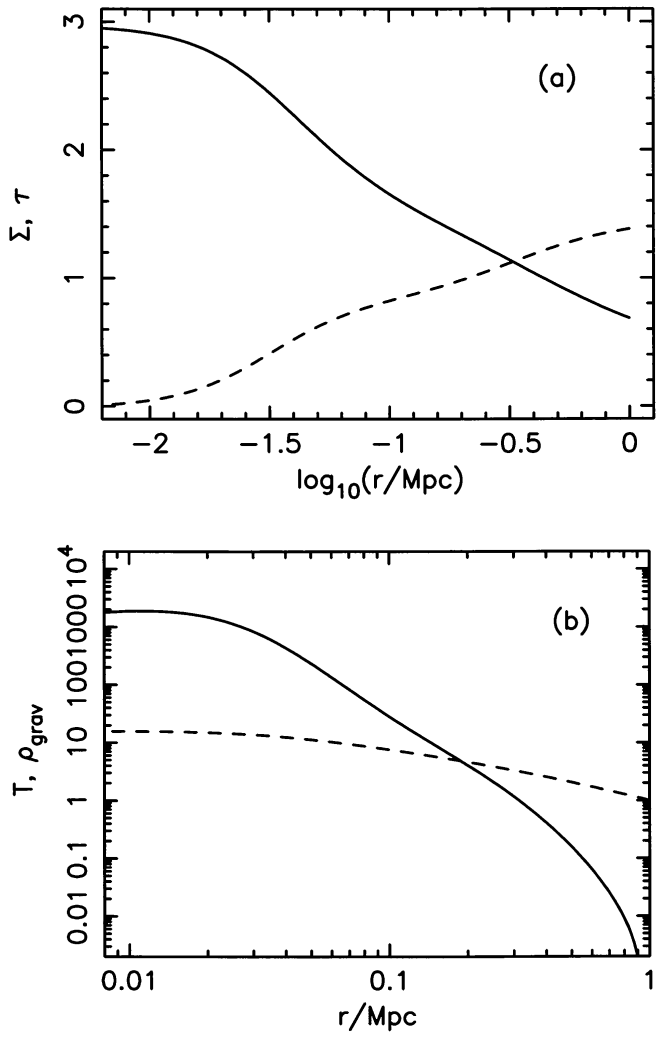

Figure 6. The $k = \infty$ cooling flow solution for PKS 0745–191: (a) Σ (dashed line) and τ (solid line), (b) the density of the gravitating matter (solid line) and the gas temperature (dashed line), in arbitrary units.

Note that the solution tends to an isothermal, constant pressure flow, with $\dot{M} \propto r^3$, within the core of the emissivity profile; this is accompanied by a flattening of the density profile of the dark matter. Unfortunately, just as for A85, high values of k give steeply rising dark matter density and temperature profiles at larger radii which seem to be incompatible with observations: Allen et al. (1996a) find the emission-weighted temperature in the inner bin of their *ASCA* data (which covers the whole of the cooling flow region) to be approximately two-thirds of that at greater radii; in our model the emission-weighted temperature from within the cooling flow region is 2.4 times greater than that at its edge.

Solutions for finite values of k fail only because of the flattening of the emissivity profile in the cluster core. The bin-widths are 8 arcsec, compared with the *ROSAT* HRI FWHM of 4 arcsec. Also, the central bin is the one most likely to be affected by uncertainties in the excess absorbing column that is required by the spectral fits. If we choose to ignore the inner bin, then it is possible to find solutions for all values of k. The dashed line in Fig. 5 shows the emissivity profile that corresponds to a mass density

$$\rho_{\rm grav} \propto \left[1 + \left(\frac{r}{0.11\,{\rm Mpc}}\right)^2\right]^{-1.57} \qquad (20)$$

and $k = 1$. The emission-weighted temperature from within the cooling flow region is now about 80 per cent of that at its edge, much

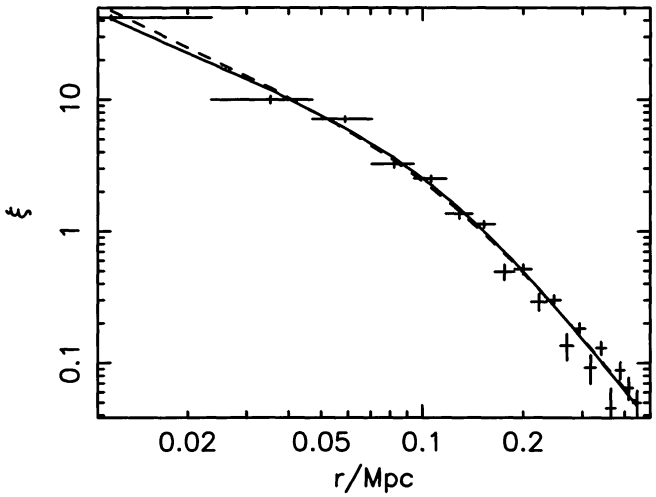

Figure 7. The emissivity profile for A2029 in 12-arcsec bins. The solid line shows an analytic fit to the data and the dashed line shows the emissivity profile corresponding to an analytic density profile, as described in the text.

more in line with the observations. Requiring a non-increasing core temperature restricts k to be less than 2 and the matter profile to be shallower than $\rho_{\rm grav} \propto r^{1.2}$ within 100 kpc.

4.4 A2029

For A2029 there are 7–9 bins of width 12 arcsec within the cooling radius, $r_{\rm cool} \approx 170$–210 kpc. The emissivity profile

$$\xi \propto \left[\left(\frac{r}{0.13\,\mathrm{Mpc}}\right)^{1.09} + \left(\frac{r}{0.13\,\mathrm{Mpc}}\right)^{3.34}\right]^{-1} \qquad (21)$$

shown in Fig. 7 is again too shallow in the central bin to support the $k = 1$ solution, but the inconsistency is this time so slight that it actually strengthens the case for $k \approx 1$ (as discussed in Section 3.2, the slope of the emissivity profile within the cluster core provides a measure of k). Fig. 8(a) shows that Σ drops to a value close to zero within 30 kpc. This indicates that the virial temperature has sunk well below the gas temperature (i.e. the flow is isobaric within this radius). This is reflected in Fig. 8(b) which shows the corresponding dark matter density profile. The latter is well-fitted at radii greater than 80 kpc by a mass density

$$\rho_{\rm grav} \propto \left[1 + \left(\frac{r}{0.14\,\mathrm{Mpc}}\right)^{3}\right]^{-1} \qquad (22)$$

but declines rapidly within this radius. Only a small change in the emissivity profile is required to generate solutions in which the gravitational mass has a constant core density, as indicated by the dashed line in Fig. 7 which reproduces the above density profile exactly.

Once again the $k = \infty$ models also generate acceptable solutions, but give temperature and dark matter density profiles that rise rapidly in to small radii. The constraint that the temperature be non-increasing to the cluster centre requires $k < 3$ and a matter profile shallower than $\rho_{\rm grav} \propto r^{1.1}$ within 100 kpc.

5 CONCLUSIONS AND DISCUSSION

I have rederived the cooling flow equations for a family of self-similar density distributions characterized by one parameter, k. Two of these in particular are expected to bound the behaviour of all possible flows.

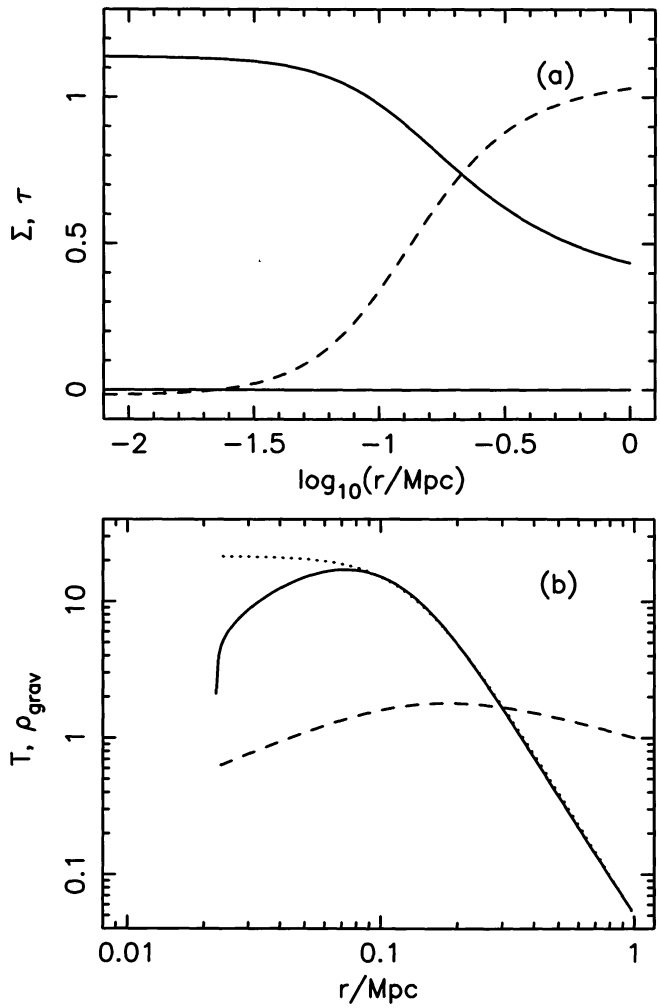

Figure 8. The $k = 1$ cooling flow solution for A2029: (a) Σ (dashed line) and τ (solid line), (b) the density of the gravitating matter (solid line), an analytic fit as described in the text (dotted line) and the temperature of the gas (dashed line).

The steady-state cooling flow equations are *not* compatible with all conceivable emissivity profiles. Thus they can be used as a test of the theory.

Given an emissivity profile and a value of k, I have shown how one can derive the gravitating mass profile, $M(r)$, and the gas temperature, $T(r)$, within the cooling radius.

I have applied my method to *ROSAT* HRI imaging data from three rich clusters.

(i) All can be fitted by models in which $k = \infty$: the corresponding distributions of dark matter have small or non-existent core radii, but have gas temperatures that rise sharply at small radii, at variance with the observations.

(ii) By contrast, models in which $k \approx 1$ give larger core radii, 110–$140\,h_{50}^{-1}$ kpc, and temperature profiles that decline towards the cluster centre (however, one of the clusters, PKS 0745–191, cannot be fitted with such a model unless the central bin of the emissivity profile is omitted from the analysis).

(iii) In every case, the requirement that the temperature gradient be non-increasing towards the cluster core places similar constraints on the solutions. The value of k must be less than about 2–3, and the matter profile must have a density gradient shallower than $\rho_{\rm grav} \propto r^{-1.2\pm0.1}$.

The X-ray surface brightness distributions of clusters of galaxies show a wide variety of core radii (Jones & Forman 1984), ranging from a few tens to a few hundreds of kpc. The optical core radii, from the galaxy distribution, are less certain: some groups find values similar to those seen in X-rays (e.g. Girardi et al. 1995 find a median value of $340\,h_{50}^{-1}$ kpc); others (e.g. Lubin & Postman 1996) find smaller values. Observations of gravitationally lensed arcs require small cores ($\lesssim 100\,h_{50}^{-1}$ kpc) in the underlying matter distribution (e.g. Wu & Hammer 1993; Miralda-Escudé & Babul 1995; Hattori, Watanabe & Yamashita 1997).

Cooling flows probe the gravitational potential deep within the cluster. For the three clusters modelled in this paper, the largest allowable core radii (for $k = 1$) are marginally consistent with the lensing results, at the lower end of optical measurements. Unfortunately, these core radii are only slightly smaller than the radii of the cooling flows. The self-similar, steady-state assumption may be a poor one at the edge of the flow (or it may be valid well beyond the cooling radius), and it is possible that models could be found that were consistent with a much larger core radius. By raising k, it is possible to find solutions with more centrally concentrated matter distributions, but at the expense of raising the temperature in the cluster core.

Ideally, one would like a much better resolution at smaller radii, so that the tendency of the emissivity profile to a constant slope, indicative of the particular value of k, could be checked. This may be possible for some of the closer clusters, such as Virgo.

Note that the solutions for Σ and τ given in this paper do not depend upon the normalizations of the gas and total gravitational masses. If desired, these can be determined by fixing the overall temperature and luminosity. The analysis of Gunn & Thomas (1996) shows that the gas density will be slightly lower and the total mass density slightly higher than in the equivalent single-phase analysis.

Cooling flows in individual galaxies are much better resolved than those in clusters, and so look like promising candidates for the kind of modelling discussed here. However, the lower temperatures lead to complications such as a varying slope, α, for the cooling function, and larger corrections for absorption and emission lying outside the pass-band of the detector. There may also be sources of mass and energy injection into the flow.

ACKNOWLEDGMENTS

I would like to thank the anonymous referee who made several useful suggestions which helped to improve the paper. The *ROSAT* HRI data were kindly supplied by Clovis Peres. This paper was prepared using the facilities of the Starlink minor node at Sussex. It was written while PAT was holding a Nuffield Foundation Science Research Fellowship.

REFERENCES

Allen S. W., Fabian A. C., Kneib J. P., 1996a, MNRAS, 279, 615
Allen S. W., Fabian A. C., Edge A. C., Bautz M. W., Furuzawa A., Tawara, Y., 1996b, MNRAS, 283, 263
Girardi M., Biviano A., Giuricin G., Madirossian F., Mezzetti M., 1995, ApJ, 438, 527
Gunn K. F., Thomas P. A., 1996, MNRAS, 281, 1133
Hattori M., Watanabe K., Yamashita K., 1997, A&A, 319, 764
Jones C., Forman W., 1984, ApJ, 276, 38
Lubin L. M., Postman M., 1996, AJ, 111, 1795
Miralda-Escudé J., Babul A., 1995, ApJ, 449, 18
Nulsen P. E. J., 1986, MNRAS, 221, 377
Nulsen P. E. J., 1988, in Fabian A. C., ed., NATO ASI, Cooling flows in clusters and galaxies. Kluwer, Dordrecht, p. 175
Pislar V., Durret F., Gerbal D., Lima Neto G. B., Slezak E., 1997, A&A, 322, 53
Thomas P. A., 1988a, in Fabian A. C., ed., NATO ASI, Cooling flows in clusters and galaxies. Kluwer, Dordrecht, p. 361
Thomas P. A., 1988b, MNRAS, 235, 315
Thomas P. A., Fabian A. C., Nulsen P. E. J. N., 1987, MNRAS, 228, 973
Waxman E., Miralda-Escudé J., 1995, ApJ, 451, 451
Wu X., Hammer F., 1993, MNRAS, 262, 187

APPENDIX A: DERIVATION OF THE MULTIPHASE COOLING FLOW EQUATIONS

We assume an emulsion of density phases which comove with the flow. The distribution is described by the volume fraction, $f(\rho, \boldsymbol{r}, t)$, such that $f\,\mathrm{d}\rho$ is the fractional volume occupied by phases with densities in the range ρ to $\rho + \mathrm{d}\rho$. Then $\int f\,\mathrm{d}\rho = 1$, and the mean density is $\bar{\rho} = \int f\rho\,\mathrm{d}\rho$.

Mass conservation gives

$$\frac{\partial}{\partial t}(\rho f) + \nabla\cdot(\boldsymbol{u}\rho f) + \frac{\partial}{\partial\rho}(\dot{\rho}\rho f) = 0, \tag{A1}$$

where $\boldsymbol{u}$ is the rate of change of position and $\dot{\rho}$ is the rate of change of density following the flow. The final term in equation (A1) is the equivalent in density space of the divergence in velocity space.

Integrating over all densities we obtain

$$\frac{\dot{\bar{\rho}}}{\bar{\rho}} + \nabla\cdot\boldsymbol{u} + \beta = 0, \tag{A2}$$

where

$$\beta \equiv \frac{1}{\bar{\rho}}\lim_{\rho\to\infty}(\dot{\rho}\rho f). \tag{A3}$$

This is equivalent to the usual single-phase equation (e.g. Thomas 1988a) except that the mass deposition rate is specified in terms of f rather than being a free parameter.

To find how the volume fraction changes with time we use the energy equation,

$$\rho\dot{s} = -n^2\Lambda, \tag{A4}$$

where s is the specific entropy and $n^2\Lambda$ is the radiated power per unit volume. For a fully ionized plasma

$$s \equiv \frac{1}{\gamma - 1}\frac{k_\mathrm{B}}{\mu m_\mathrm{H}}\ln\left(\frac{P}{\rho^\gamma}\right), \tag{A5}$$

where P is the pressure, k_B is the Boltzmann constant, μm_H is the mass per particle and $\gamma = 5/3$. Then

$$\frac{\dot{\rho}}{\rho} = \frac{1}{\gamma}\frac{\dot{P}}{P} + \frac{\gamma - 1}{\gamma}\frac{n^2\Lambda}{P}. \tag{A6}$$

Over a wide temperature range appropriate to clusters, the cooling function can be approximated by a power law, $\Lambda \propto T^\alpha$, where $\alpha \approx 0.5$. Then equation (A6) can be simplified by moving to a new density variable. Writing

$$\rho = \rho_0(\boldsymbol{r}, t)w^{-1/(2-\alpha)}, \tag{A7}$$

we obtain

$$\dot{w} = (2-\alpha)\left(\frac{\dot{\rho}_0}{\rho_0} - \frac{1}{\gamma}\frac{\dot{P}}{P}\right)w - (2-\alpha)\frac{\gamma - 1}{\gamma}\frac{n_0^2\Lambda(T_0)}{P}. \tag{A8}$$

If the adiabatic compression term is removed by setting $P \propto \rho_0^\gamma$, then the energy equation takes a particularly simple form, $\dot{w}$ =constant. However, a more useful choice is to take $\rho_0 \propto \bar{\rho}$. From the final term

of equation (A1), we see that at high density when cooling is dominant then $\dot{\rho}\rho f \sim$ constant. This motivates the substitution

$$f = \frac{(2-\alpha)}{\rho_0} w^{(4-\alpha)/(2-\alpha)} g(w, \boldsymbol{r}, t). \tag{A9}$$

Then using equations (A1), (A6) and (A8) we obtain the following equation for the covariant derivate of g (i.e. following the fluid flow):

$$\frac{\dot{g}}{g} + (3-\alpha)\frac{\dot{\rho}_0}{\rho_0} - \frac{2-\alpha}{\gamma}\frac{\dot{P}}{P} + \nabla \cdot \boldsymbol{u} = 0. \tag{A10}$$

This paper has been typeset from a TEX/LATEX file prepared by the author.